Supporting Information

Adsorption Contraction Mechanics: Understanding Breathing Energetics in Isoreticular Metal–Organic Frameworks

Simon Krause[‡,a], Jack D. Evans[‡,a,b], Volodymyr Bon[a], Irena Senkovska[a], Sebastian Ehrling[a], Ulrich Stoeck[a], Pascal G. Yot[c], Paul Iacomi[d], Philip Llewellyn[d], Guillaume Maurin[c], François-Xavier Coudert[b] and Stefan Kaskel[,a]*

[a] Department of Inorganic Chemistry, Technische Universität Dresden, Bergstrasse 66, 01062 Dresden, Germany

[b] Chimie ParisTech, PSL Research University, CNRS, Institut de Recherche de Chimie, Paris, 75005 Paris, France.

[c] Institut Charles Gerhardt Montpellier UMR 5253 CNRS UM ENSCM, Université de Montpellier. Place E. Bataillon, 34095 Montpellier cedex 05, France

[d] Aix-Marseille Univ., CNRS, MADIREL (UMR 7246), 13013 Marseille, France

*E-mail: stefan.kaskel@tu-dresden.de

1 Methods and Materials

Materials and gases used in the synthesis and analysis of ligands, DUT-49, and DUT-48 samples were of high purity. $Cu(NO_3)_2 \cdot 3H_2O$ (Sigma Aldrich, 99.5%), acetic acid (AcOH) (AppliChem, 99%), (*N*-methyl-2-pyrrolidone (NMP) (AppliChem, 99%), *N,N* Dimethylformamide (DMF) (Fischer Scientific, 99%), anhyd. ethanol (VWR Prolabo, 99%) were used for the synthesis and activation of DUT-49 ($C_{40}H_{20}N_2O_8Cu_2$) and DUT-48. The ligand H_4bbcdc (9,9'-([1,1'-biphenyl]-4,4'-diyl)bis(9*H*-carbazole-3,6-dicarboxylic acid)) incorporated in DUT-49 was used following a previously reported study by our group[1]. The synthetic protocol and analytic data can be obtained from reference 1.

Powder X-ray diffraction (PXRD) patterns were collected in transmission geometry with a STOE STADI P diffractometer operated at 40 kV and 30 mA, with monochromatic Cu-$K_{\alpha 1}$ (λ = 0.15405 nm) radiation, a scan speed of 20 s per step and a step size of 0.1° 2Θ. Activated samples were prepared under inert atmosphere.

Thermogravimetric analysis (TGA) was carried out in synthetic dry air using a NETZSCH STA 409 thermal analyzer at a heating rate of 5 K min^{-1}.

Elemental analysis (C, H, N, S) was performed for ligand and MOF materials with a HEKATECH EA 3000 Euro Vector CHNS analyzer.

Scanning electron microscopy (SEM) images of DUT-49 and DUT-48 were taken with secondary electrons in a HITACHI SU8020 microscope using 1.0 kV acceleration voltage and 10.8 mm working distance. The powdered samples were prepared on a sticky carbon sample holder under inert atmosphere.

Volumetric adsorption experiments were carried out on a BELSORP-max instrument and gases with high purity were used (N_2: 99.999%, *n*-butane: 99.95%, He: 99.999%, CH_4: 99.999%,). For volumetric adsorption experiments the measuring routine of BELSORP-max was used. Targeted relative pressures in the range of 0.001 – 100 kPa were defined and limits of excess and allowance amount were set to 10 and 20 $cm^3\ g^{-1}$, respectively. For high resolution isotherms of *n*-butane limits of excess and allowance amount were set to 2 and 4 $cm^3\ g^{-1}$, respectively. Equilibration conditions for each point were set to: 1% pressure change within 350 s. The dead volume was routinely determined using helium. Values for the adsorbed amount of gas in the framework are all given at standard temperature and pressure (STP), except the high pressure measurements. Liquid nitrogen was used as coolant for measurements at 77 K and a Julabo thermostat was used for measurements at 298 K. Measurements at 111 K and 121 K were carried out using a closed cycle He-cryostat setup described in reference [1]. Samples of DUT-48 and DUT-49 were installed in the measuring set up under inert atmosphere.

High pressure H_2 adsorption measurement at 77 K up to 110 bar was performed on a volumetric BELSORP-HP apparatus. High pressure CH_4 and CO_2 adsorption was studied using a magnetic suspension balance (Rubotherm Co.). The total gas uptake was calculated as follow: $N_{total} = N_{excess} + \rho_{bulk} V_{pore}$, where ρ_{bulk} equals to the density of compressed gases at the measuring temperature and pressure, and V_{pore} was obtained from the N_2 sorption isotherm at 77 K.

2 Synthesis of H_4pbcdc (9,9'-(1,4-Phenylene)bis(9*H*-carbazole-3,6-dicarboxylic acid))

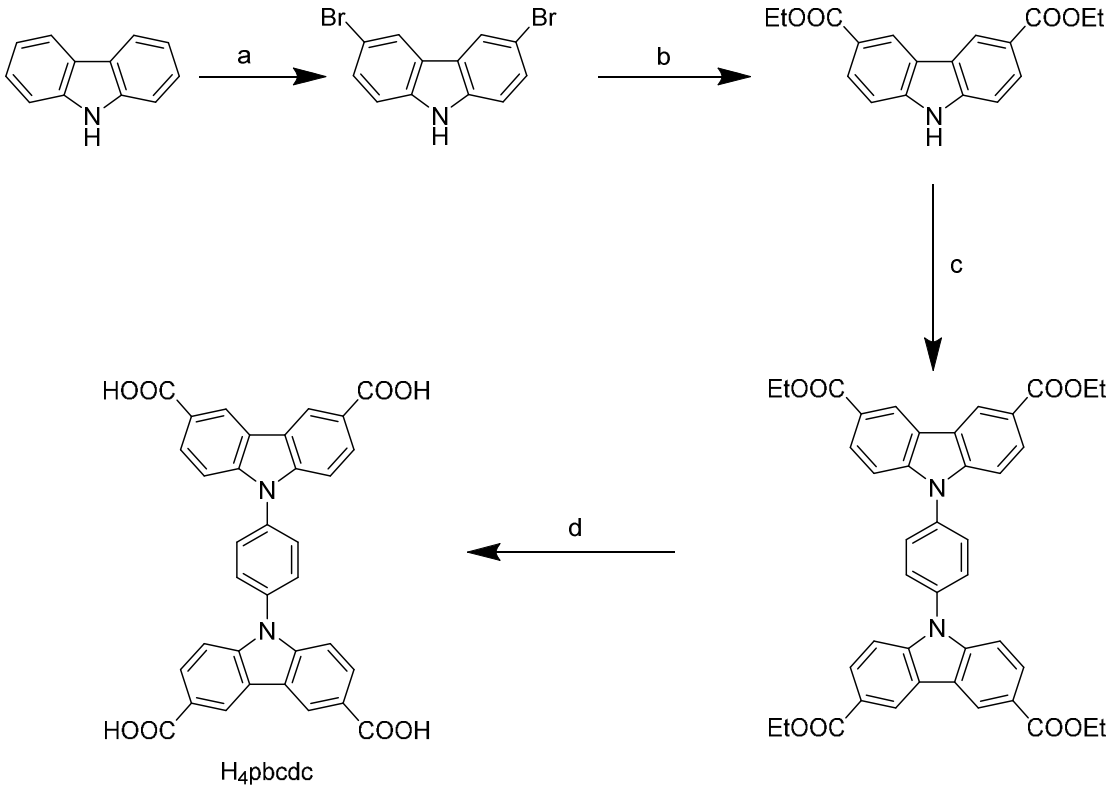

Scheme S 1. Synthesis of H_4pbcdc a) N-Bromosuccinimide, THF, 40 °C, 20 h. b) 1. *n*-butyllithium, trimethylsilyl chloride, diethyl ether, -78 °C, 1 h; 2. *tert*-butyllithium, *-78 °C*, 2h, CO_2, 20min. c) 1,4 Diiodobenzene, CuI, L-proline, K_2CO_3, DMSO, 90 °C, 48 h. d) KOH, THF/H_2O/MeOH, 60 °C, 24 h.

2.1 3,6-Dibromo-9*H*-carbazole

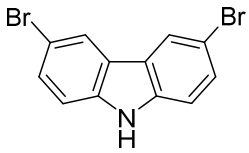

To a solution of 150 g (0.9 mol) 9*H*-carbazole in 2 l of THF 351 mg (1.97 mol) *N*-bromosuccinimide are slowly being added at 40 °C over 30 min. The light brown solution is stirred over 20 h at 40 °C. Afterwards the THF is being removed in vacuum and the solid washed thoroughly with water. The resulting pale white solid is recrystallized in a mixture of Dichloromethane (DCM) and *n*-hexane to yield 209.9 g (0.65 mol, 75%) of the pure white product.

Elemental analysis: $C_{12}H_7Br_2N$ (325.00 g mol^{-1})

calculated:	C: 44.35 %	H: 2.17 %	N: 4.34 %	Br. 49.17 %.
experimental:	C: 44.27 %	H: 2.09 %	N: 4.41 %	

2.2 Diethyl 9*H*-carbazole-3,6-dicarboxylate

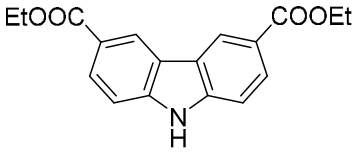

In a dried SCHLENK flask 26.5 g (58.8 mmol) 3,6-dibromo-9*H*-carbazole are dissolved 950 ml in diethyl ether at 0 °C under Ar-atmosphere. To the solution 35 ml of a 2.5 M n-butyllithium solution in *n*-hexane were slowly added over 30 min, the solution stirred for 1 h at 0 °C and 11.1 ml of trimethylsilyl chloride were slowly added over 10 min. The suspension was stirred for 1 h at 0 °C, cooled to -78 °C and 202 ml of a 1.7 M tert butyllithium solution in pentane were added over 40 min. After stirring the solution for 2 h at -78 °C dry CO_2 was bubbled through through the reaction mixture for 20 min. the reaction mixture was allowed to warm to room temperature overnight. The white suspension was quenched with 50 ml water and the diethylether was removed in vacuum. The resulting suspension was stirred in 500 ml 1 M hydrochloric acid at 90 °C, filtered and dried at 80 °C. The off white product was suspended in 1 l ethanol, 2 ml of concentrated sulfuric acid were added and the suspension was stirred under reflux for 24 h. The ethanol was removed in vacuum, the resulting solid dissolved in ethylacetate and washed with saturated sodium carbonate solution. The organic solution was dried over $MgSO_4$ and the solvent removed in vacuum. The solid was purified by chromatography in a DCM/ethylacetate mixture of 15:1 to yield 12.27 g ester.

^{1}H-NMR (600 MHz, d_6-DMSO):

δ (in ppm) = 1.37 (tr, J = 7.0 Hz, 6H), 4.35 (q, J = 7.0 Hz, 4H), 7.61 (dd, J = 8.5 Hz, J = 0.6 Hz, 2H), 8.06 (dd, J = 8.5 Hz, J = 1.7, 2H), 8.89 (dd, J = 1.7 Hz, J = 0.6 Hz, 2H), 12.09 (s, 1H).

^{13}C-NMR und DEPT (150 MHz, d_6-DMSO):

δ (in ppm) = 14.38 (CH_3), 60.39 (CH_2), 111.31 (CH), 121.24 (Cq), 122.29 (Cq), 122.77 (CH), 127.46 (CH), 143.25 (Cq), 166.33 (Cq).

Elemental analysis: $C_{18}H_{17}NO_4$ (311.33 g mol^{-1})

calculated:	C: 69.44 %	H: 5.50 %	N: 4.50 %.
experimental:	C: 69.71 %	H: 5.63 %	N: 4.37 %.

2.3 9,9'-(1,4 Phenylen)bis(3,6-diethoxycarbonyl)carbazol

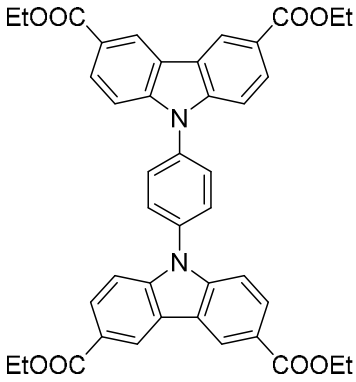

In a SCHLENK tube 6 g (19.27 mmol) 3,6-diethoxycarbonylcarbazole, 2.89 g (8.76 mmol) 1,4 diiodbenzene, 334 mg (1.75 mmol) copper(I)iodine, 403 mg (3.5 mmol) L-proline and 4,84 g (35 mmol) potassium carbonate are dissolved in 80 ml of DMSO under inert atmosphere. The suspension is subsequently degassed by dynamic vacuum at 10^{-2} mbar and heated to 90 °C for two days. After addition of 300 ml water and 2 ml 2M hydrochloric acid the precipitate was filtered off, washed with water and dissolved in DCM. The DCM solution was extracted with water, the organic solution dried over $MgSO_4$ and removed in vacuum. The obtained off white powder was recrystallized from ethyl acetate to obtain 4.58 g (6.57 mmol, 75 %) white powder.

^{1}H-NMR (600 MHz, $CDCl_3$):

δ (in ppm) = 1.49 (tr, J = 7.3 Hz, 12H), 4.48 (q, J = 7.3 Hz, 8H), 7.56 (d, J = 8.5 Hz, 4H), 7.88 (s, 4H), 8.23 (dd, J = 8.5 Hz, J = 1.6 Hz, 4H), 8.97 (d, J = 1.6 Hz, 4H).

Elemental analysis: $C_{42}H_{36}N_2O_8$ (696.74 g mol^{-1})

calculated:	C: 72.40 %	H: 5.21 %	N: 4.02 %.
experimental:	C: 72.49 %	H: 5.33 %	N: 4.03 %.

2.4 9,9'-(1,4-Phenylen)biscarbazol-3,6-dicarboxylic acid

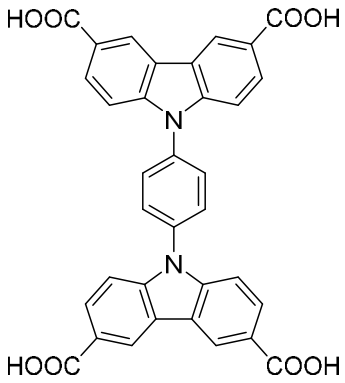

4 g (5.74 mmol) 9,9'-(1,4 phenylen)bis(3,6-diethoxycarbonyl)carbazole are dissolved in a solvent mixture of 100 ml THF, 50 ml methanol and 50 ml water at 60 °C. To the solution 1.93 g (34.44 mmol) potassiumhydroxide were added and the solution was stirred for 24 h at 60 °C, the organic solvents were then removed in vacuum and the solution diluted with 50 ml water. The pH was adjusted to 4 by addition of 2M hydrochloric acid and a white precipitate was formed which was filtered off, washed 3 times with fresh water and dried at 80 °C to obtain 3.33 g (5.7 mmol, 99%) of the pure product as white powder

^{1}H-NMR (600 MHz, d_6-DMSO):

δ (in ppm) = 7,69 (d, J = 8.5 Hz, 4H), 8.04 (s, 4H), 8.16 (dd, J = 8.5 Hz, J = 1.3 Hz, 4H), 9.03 (d, J = 1.3 Hz, 4H), 12.88 (s br, 4H).

^{13}C-NMR und DEPT (150 MHz, d_6-DMSO):

δ (in ppm) = 110.06 (CH), 123.10 (Cq), 123.54 (CH), 124.07 (Cq), 128.78 (CH), 129.38 (CH), 136.03 (Cq), 143.88 (Cq), 168.09 (Cq).

Elemental analysis: $C_{34}H_20N_2O_8$ (584.53 g mol^{-1})

calculated:	C: 69.86 %	H: 3.45 %	N: 4.79 %.
experimental:	C: 69.76 %	H: 3.41 %	N: 4.62 %.

3 Synthesis of H_4bbcdc (9,9'-([1,1'-biphenyl]-4,4'-diyl)bis(9H-carbazole-3,6-dicarboxylic acid))

The ligand H_4bbcdc (9,9'-([1,1'-biphenyl]-4,4'-diyl)bis(9*H*-carbazole-3,6-dicarboxylic acid)) was used from a synthesis previously reported by our group. The synthetic protocol including the analytic data can be obtained from reference 1.

4 Synthesis of DUT-48 and DUT-49 samples

For the described experiments DUT-48 and DUT-49 were synthesized on larger scale based on a solvothermal reaction of the regarding ligands with $Cu(NO_3)_2 \cdot 3H_2O$ in NMP at 80 °C for 48 h similar to what has been previously described for DUT-49 in reference[1]. The synthesis conditions for PCN-81 were used in a second synthesis according to reference 2. In addition, a synthetic approach using larger amounts of DMF and acetic acid to avoid reduction of the Cu^{2+} by NMP was used. All reaction conditions and yields are listed in Table S1.

Table S1 Conditions used for the synthesis of DUT-48

Reference	$m_{Cu(NO3)2 \cdot 3H2O}$ (mg)	m_{Ligand} (mg)	modulator	solvent	*T* (°C)	$t_{reaction}$ (h)	Yield (%)[a]
2	2440	840	1.68 ml 48% HBF_4	84 ml DMSO + 168 ml DMA	85	96	52
This work	515	500	AcOH 2.5 ml	NMP 450 ml	80	24	64
This work	1030	1000	AcOH 12 ml	DMF 800 ml	80	72	51

[a]based on the amount of ligand, determined after activation, actual yield of reaction is larger

PXRD patterns obtained for the reaction products are given in Figure S1-Figure S7, N_2 adsorption isotherms at 77 K are given in Figure S12. Due to the best adsorption performance of DUT-48(3) all further adsorption and Hg-intrusion experiments were carried on this sample.

5 Washing and activation of DUT-48 and DUT-49 Samples

The blue precipitates obtained after the solvothermal synthesis of DUT-48 and DUT-49 (conditions under Table S1) were washed 6 times with fresh DMF over a period of two days at room temperature. The NMP was exchanged by anhydr. ethanol 10 times over 4 days. The respective blue precipitates of DUT-48 and DUT-49 were subjected to an activation procedure involving supercritical CO_2 previously described for DUT-49[3]: The samples which were suspended in ethanol were placed in filter frits into a Jumbo Critical Point Dryer 13200J AB (SPI Supplies) which was subsequently filled with liquid CO_2 (99.995% purity) at 15 °C and 50 bar. To ensure a complete substitution of ethanol by CO_2, the liquid in the autoclave was exchanged with fresh CO_2 18 times over a period of 5 days. The temperature and pressure were then risen beyond the supercritical point of CO_2 (35 °C and 100 bar) and kept until the temperature and pressure was constant at least for 1 h. The supercritical CO_2 was steadily released over 3 h. The dry powder was further subjected to additional thermal activation by heating the sample under dynamic vacuum ($p < 10^{-3}$ mbar) at 100 °C for 24 h. The dark blue powders were transferred and stored in an argon filled glove box (H_2O content < 1 ppm).

6 Characterization of DUT-48 and DUT-49

6.1 Powder X-ray Diffraction

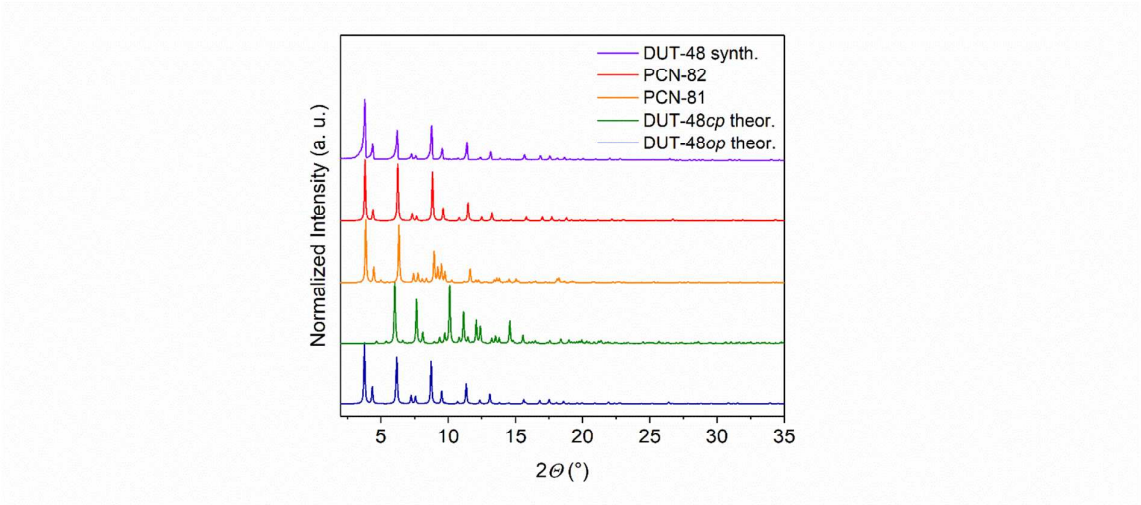

Figure S1. PXRD patterns calculated for DUT-48op (blue), DUT-48cp (green), PCN-81 (orange), PCN-82 (red), and experimental pattern for activated DUT-48(purple) from bottom to top, respectively.

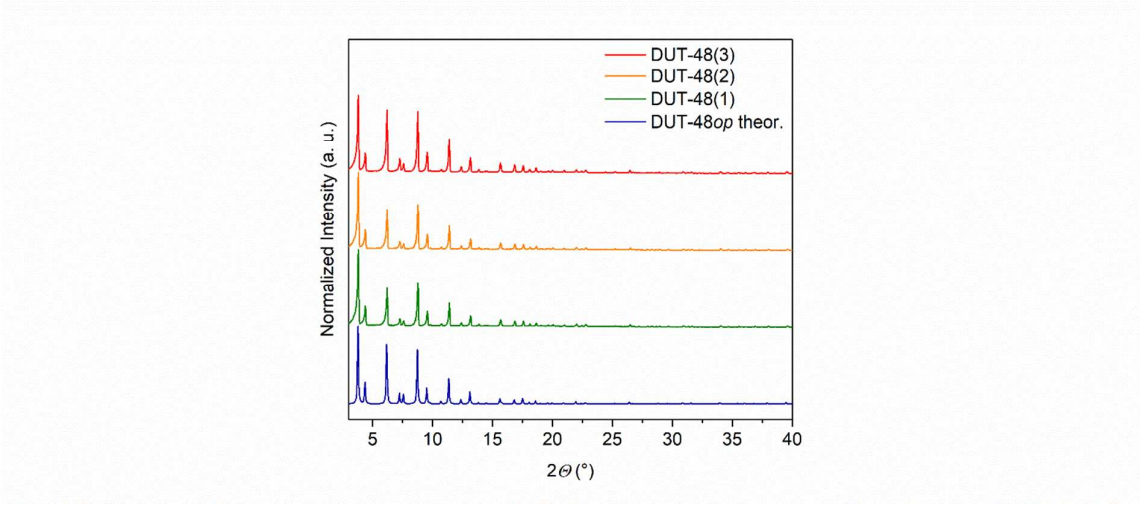

Figure S2. PXRD patterns calculated for DUT-48op (blue), activated DUT-48(1) (green), activated DUT-48(2) (orange), activated DUT-48(3) (red), from bottom to top, respectively.

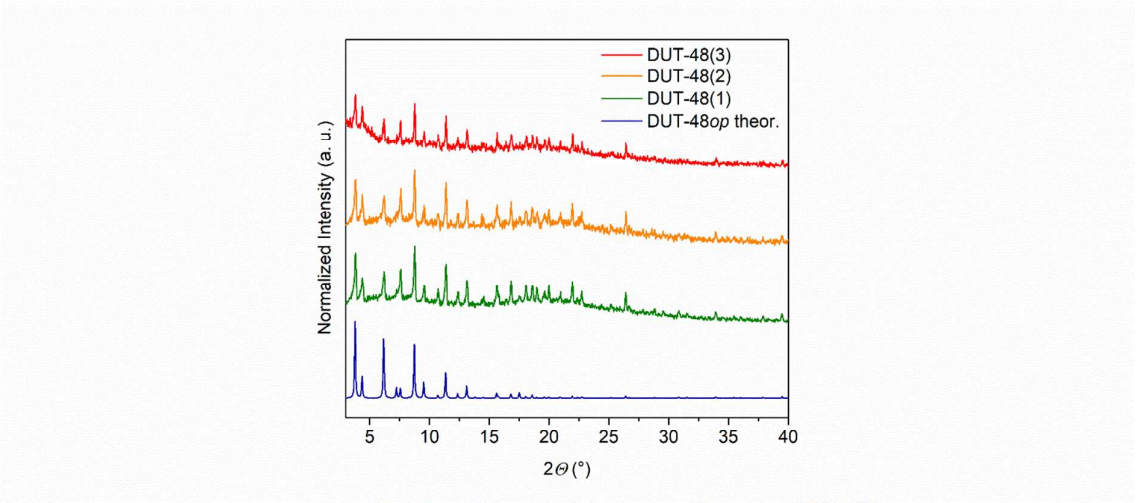

Figure S3. PXRD patterns calculated for DUT-48op (blue), as made DUT-48(1) (green), as made DUT-48(2) (orange), as made DUT-48(3) (red), from bottom to top, respectively.

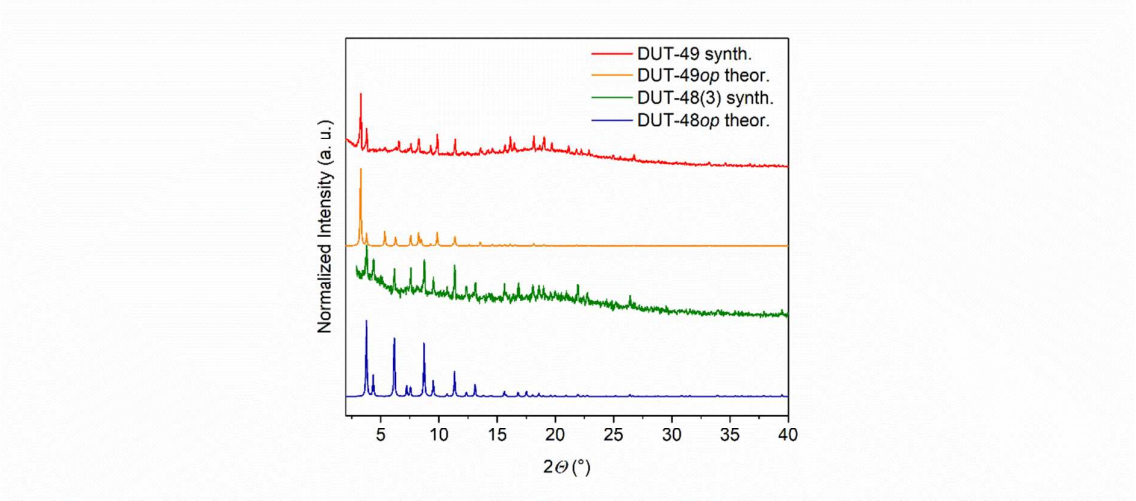

Figure S4. PXRD patterns calculated for DUT-48*op* (blue), as made DUT-48(3) (green), calculated for DUT-49op (orange), as made DUT-49 (red), from bottom to top, respectively.

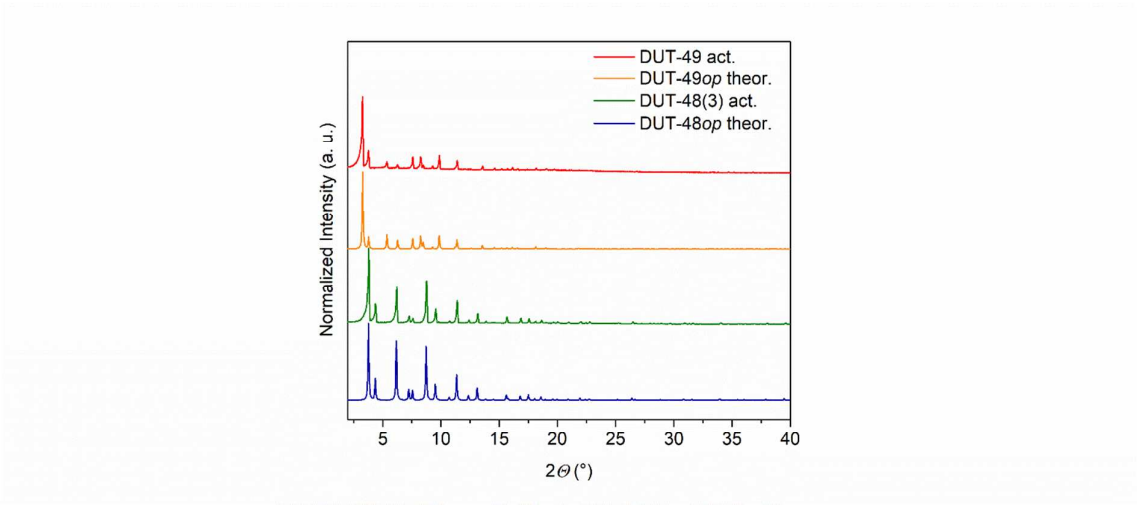

Figure S5 PXRD patterns calculated for DUT-48op (blue), activated DUT-48(3) (green), calculated for DUT-49op (orange), activated DUT-49 (red), from bottom to top, respectively.

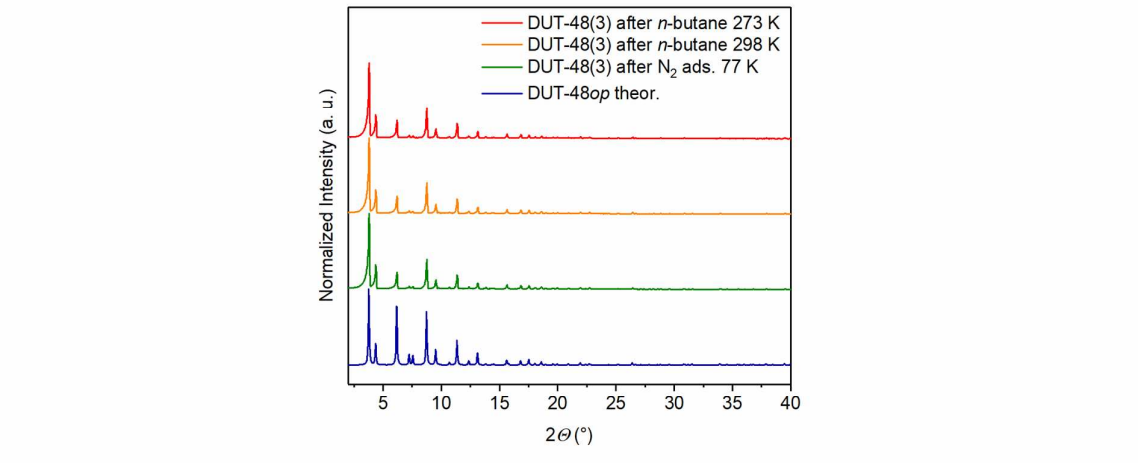

Figure 6. PXRD patterns calculated for DUT-48op (blue), experimental for DUT-48(3) after adsorption-desorption of nitrogen at 77 K (green), experimental for DUT-48(3) after adsorption-desorption of n-butane at 298 K (orange), experimental for DUT-48(3) after adsorption-desorption of n-butane at 273 K (red), from bottom to top, respectively.

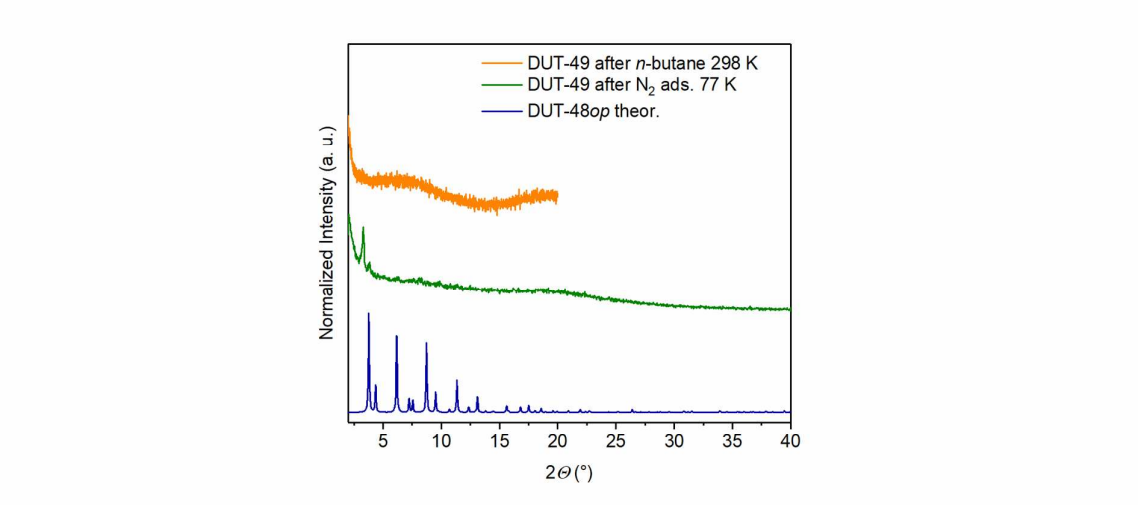

Figure S7. PXRD patterns calculated for DUT-49op (blue), experimental for DUT-49 after adsorption-desorption of nitrogen at 77 K (green), experimental for DUT-49 after adsorption-desorption of n-butane at 298 K (orange) from bottom to top, respectively.

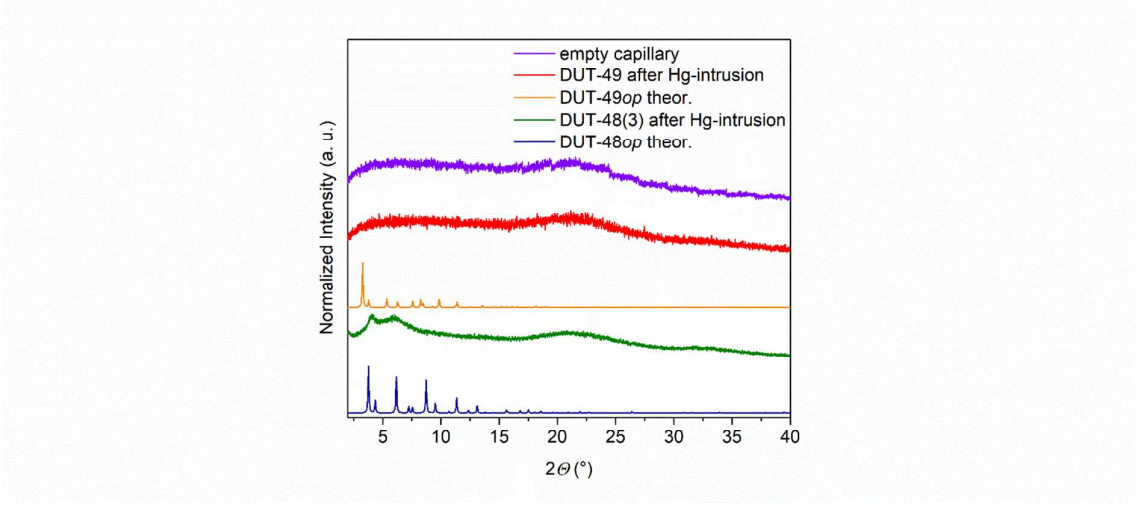

Figure S8. PXRD patterns calculated for DUT-48op (blue), experimental for DUT-48(3) after Hg-intrusion (green), calculated for DUT-49op (orange), experimental for DUT-49 after Hg-intrusion (red) and empty capillary (purple) from bottom to top, respectively.

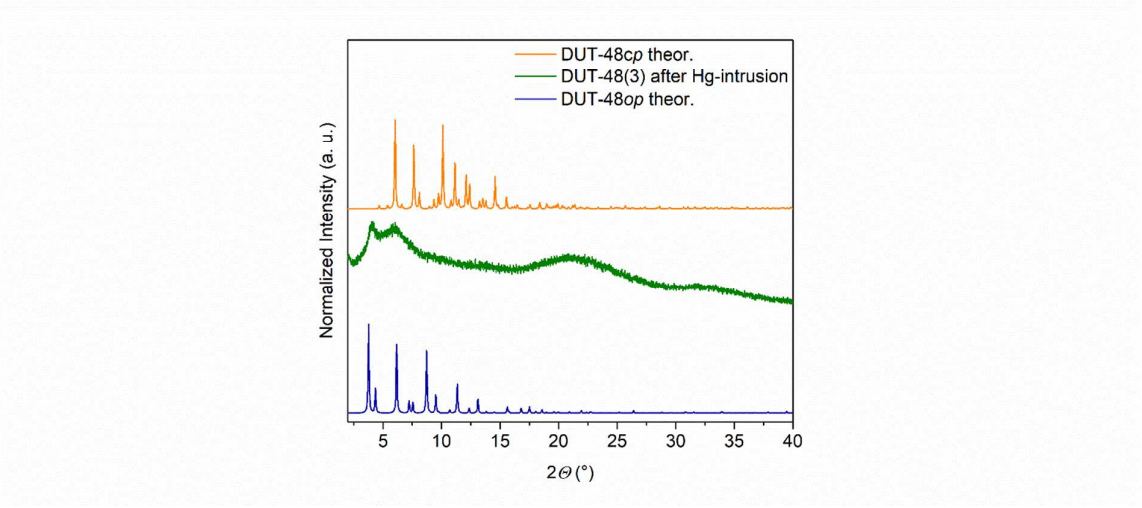

Figure S9. PXRD patterns calculated for DUT-48op (blue), DUT-48(3) after Hg-intrusion (green) and calculated for DUT-48cp theor (orange).

6.2 Single crystal X-ray diffraction

Cubic single crystal of DUT-48 was prepared in the closed glass capillary (d = 0.3 mm) with small amount of the mother liqueur. The capillary was mounted on the 1-axis goniometer of BL14.2 beamline of the MX-facility at BESSY-II synchrotron, operated by Helmholtz-Zentrum Berlin für Materialien und Energie[4]. The beamline is equipped with 1-axis goniometer and MX-225 CCD detector from Rayonix. All diffraction experiments were performed at room temperature using synchrotron radiation with E = 14 keV (λ = 0.88561 Å). The φ-scan with oscillation range of 1° was used for data collection. The diffraction images were processed using CCP4 software.[5] The crystal structure was solved by direct methods and refined by full matrix least-squares on F^2 using SHELX-2016/4 program package[6]. All non-hydrogen atoms were refined in anisotropic approximation. Hydrogen atoms were refined in geometrically calculated positions using "riding model" with $U_{iso}(H)=1.2U_{iso}(C)$. Atom C9 shows disorder by symmetry near the mirror plane and therefore was treated with occupancy factor 0.5. High symmetry of the crystal system as well as mobility of the solvent molecules in the pores make the localization of the guest molecules impossible, therefore the SQUEEZE procedure was applied to the dataset in order to correct reflection intensities, corresponding to disordered solvent molecules[7]. CCDC-1827897 contains the supplementary crystallographic data for DUT-48. This data can be obtained free of charge from the Cambridge Crystallographic Data Centre via www.ccdc.cam.ac.uk/data_request/cif

Table S2 Crystallographic data for DUT-48 and PCN-81.

	DUT-48*op*	**PCN-81(Reference 2)**
Empirical formula	$C_{34}H_{20}Cu_2N_2O_{10}$	$C_{34}H_{20}Cu_2N_2O_{10}$
Formula weight, g mol^{-1}	743.60	743.60
Crystal system, space group	cubic, $Fm\bar{3}m$	cubic, $Pa\bar{3}$
Unit cell dimensions, Å	a = 40.490(5)	a = 39.4840(16)
Volume, Å^3	66381(23)	61555(4)
Z	24	24
Calculated density, g·cm^{-3}	0.444	0.481
Temperature, K	296	173
Wavelength, Å	0.88561	0.41328
Absorption coefficient, mm^{-1}	0.728	0.230
F(000)	8928 (after SQUEEZE)	9024 (after SQUEEZE)
	$-42 \le h \le 40$	$-49 \le h \le 25$
Limiting indices	$-48 \le k \le 50$	$-43 \le k \le 49$
	$-50 \le l \le 12$	$-47 \le l \le 49$
Reflections collected / unique	40089 / 3870	543624 / 21027
R_{int}	0.0700	0.0945
Data / parameters	3870 / 84	21027 / 433
GooF on F^2	1.121	1.236
Final R indices [$I>2\sigma(I)$]	0.0748	0.1125
wR indices (all data)	0.2286	0.2983
Largest diff. peak / hole, eÅ^{-3}	1.273 / -1.376	1.134 / -1.849

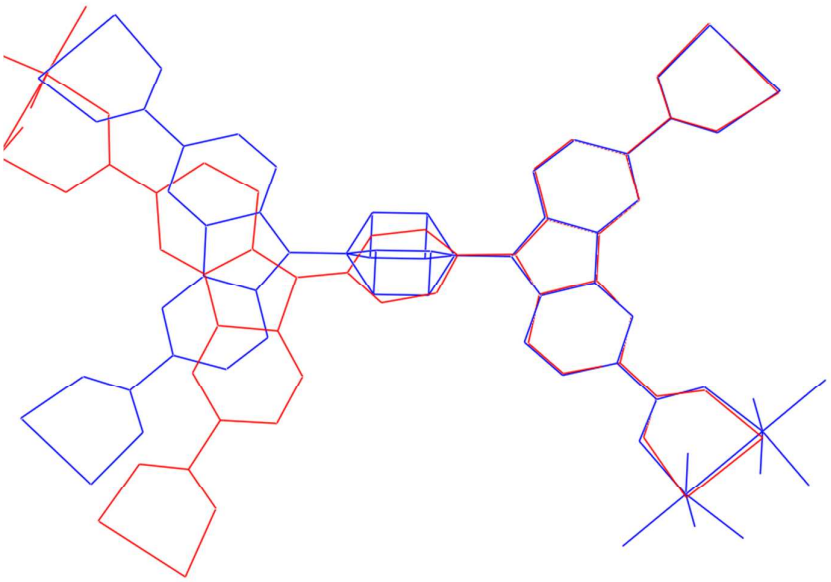

Figure S10. Comparison of linker configuration in PCN-81 (red) and DUT-48 (blue).

6.3 Thermogravimetric analysis

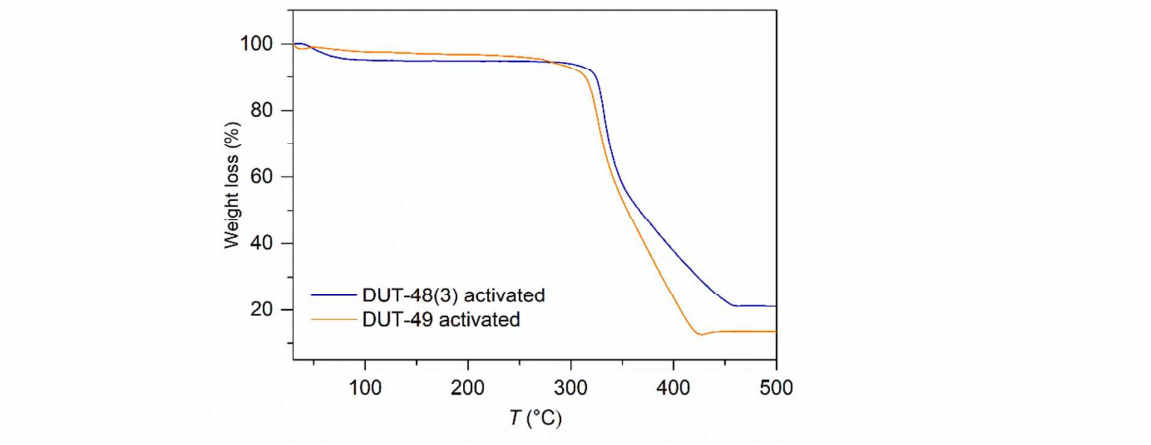

Figure S11. Thermogravimetric analysis *of activated DUT-48(3) (blue) and DUT-49 (orange)*

6.4 Elemental Analysis

The DUT-49 samples used in this study were taken from synthesis previously reported by our group.

Elemental analysis DUT-48 activated: $Cu_2C_{34}H_{16}N_2O_8$ (707.59 g mol^{-1})

calculated: C: 57.71% H: 2.28 % N: 3.96 %. O: 18.09 Cu: 17.96.

experimental: C: 56.93 % H: 2.07 % N: 3.91 %

6.5 Gas Adsorption Experiments

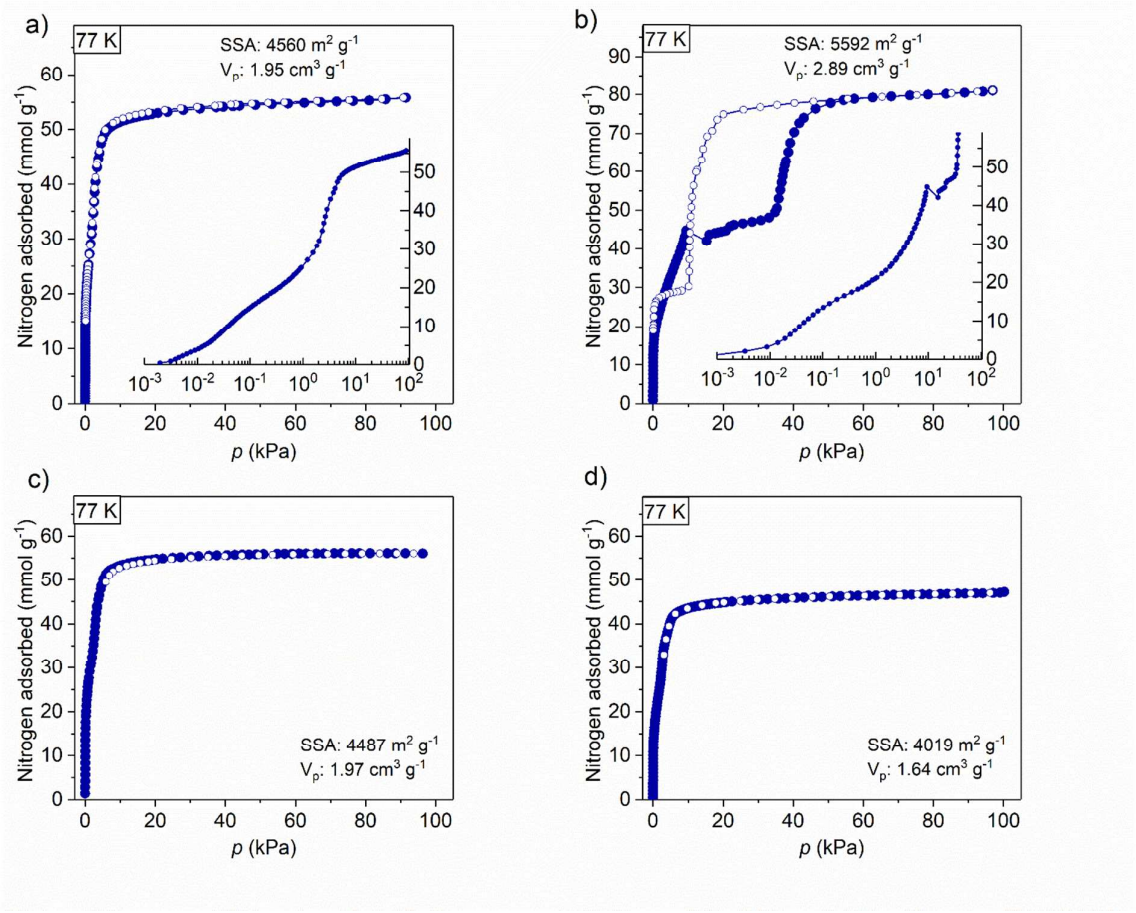

Figure S12. Nitrogen adsorption-desorption isotherms at 77 K for DUT-48(3) including inset with semilogarithmic plot (a), DUT-49 including inset with semilogarithmic plot (b), DUT-48(2) (c), and DUT-48(1) (d), closed symbols adsorption, open symbols desorption

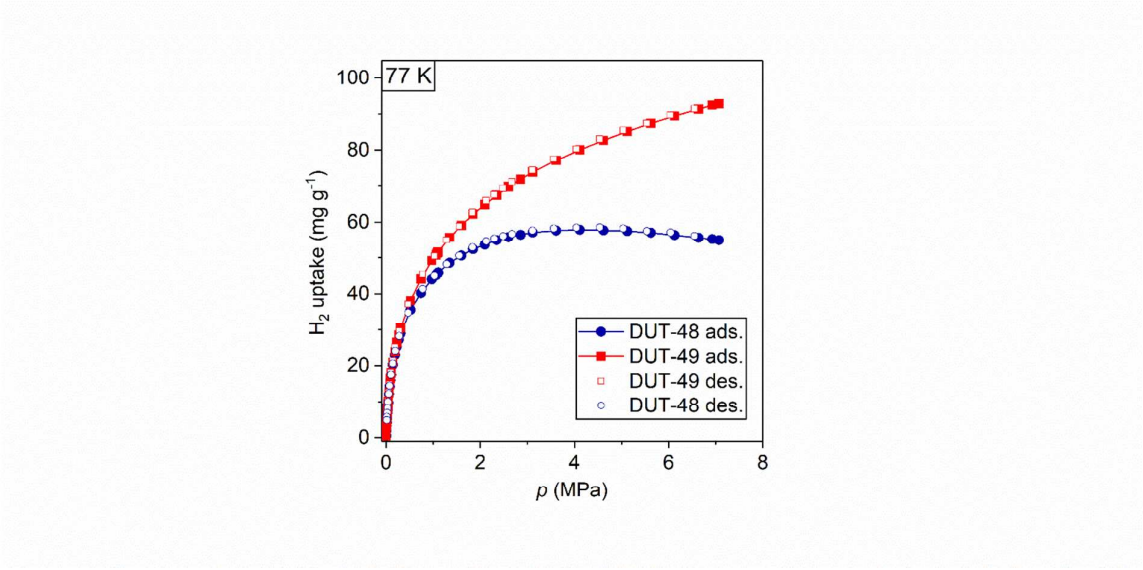

Figure S13. Hydrogen high pressure excess adsorption (filled symbols) and desorption (empty symbols) isotherm of DUT-48(3) (blue) and DUT-49 (red) at 77 K.

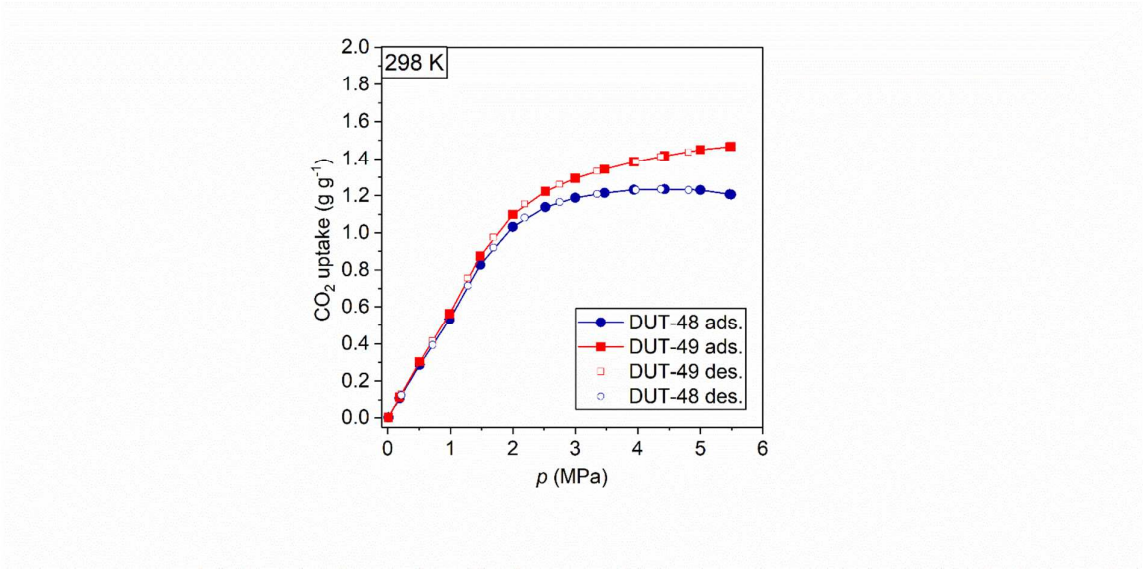

Figure S14. CO_2 high pressure excess adsorption (filled symbols) and desorption (empty symbols) isotherm of DUT-48(3) (blue) and DUT-49 (red) at 298 K.

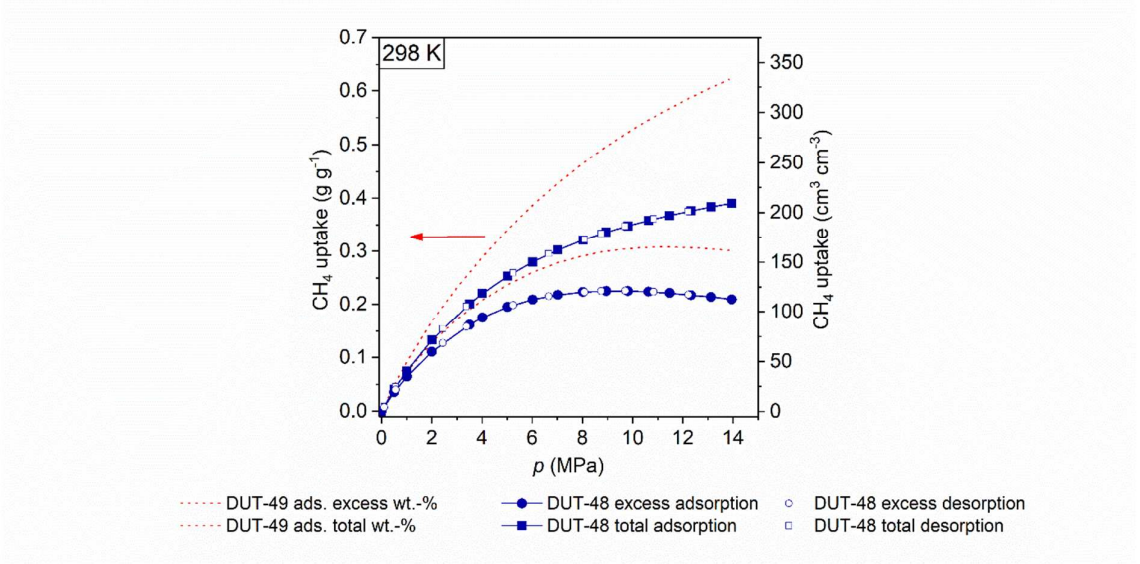

Figure S15. Methane high pressure excess (circles) and total (squares) adsorption (filled symbols) and desorption (empty symbols) isotherm of DUT-48 at 298 K. Gravimetric methane high pressure excess and total (red) adsorption isotherms for DUT-49 are shown as dashed lines and only corresponds to the values displayed on the left y-axis.

7 Enthalpy of adsorption

For microcalorimetric experiments, all isotherms and enthalpies were measured using a Tian-Calvet type microcalorimeter coupled with a home-made manometric gas dosing system[8]. This apparatus allows the simultaneous measurement of the adsorption isotherm and the corresponding differential enthalpies. Gas is introduced into the system using a step-by-step method and each dose is allowed to stabilize in a reference volume before being brought into contact with the adsorbent located in the microcalorimeter. The introduction of the adsorbate to the sample is accompanied by an exothermic thermal signal, measured by the thermopiles of the microcalorimeter. The peak in the calorimetric signal is integrated over time to give the total energy released during this adsorption step. At low coverage the error in the signal can be estimated to around ± 0.2 kJ mol^{-1}. Around 400 mg of sample is used in each experiment. For each injection of gas, equilibrium was assumed to have been reached after 90 minutes. This was confirmed by the return of the calorimetric signal to its baseline (<5 µW). The gases used for the adsorption were obtained from Air Liquide and were of minimum N47 quality (99.997 % purity).

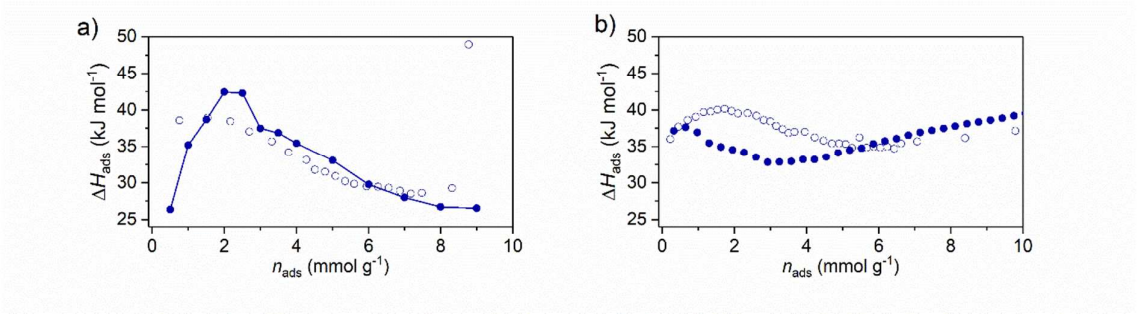

Figure S16. Isosteric adsorption enthalpy determined by the VAN'T HOFF equation (filled symbols) and by in situ calorimetry (empty symbols) for DUT-49 (a) and DUT-48 (b).

8 Hg-intrusion experiments

Mercury intrusion experiments were performed on a Hg-porosimeter Micromeritics Autopore 9240 (P≤413 MPa)) to explore the pressure-induced structural contraction of the DUT-48 and -49. The intruded volume of mercury (which is assumed to not penetrate the mesoporosity of both solids) corresponds to the volume compressed under hydrostatic conditions. The powder was previously activated under secondary vacuum at 150°C for 8 hours to obtain the large pore version of the materials as starting form. The obtained activated powders were transferred into a glove box (Jacomex, P-BOX under argon atmosphere, H_2O<5 ppm, O_2<5 ppm) where the samples were loaded into a penetrometer (Type 14 Micromeritics, 3 Bulb, 0.4120 mL stem and 3.1126 mL total volume powder penetrometer). Before the experiment the cell was then evacuated under primary vacuum to outgas the argon for 10 minutes.

The resulting volume of the phase obtained after compression can be extracted from the cumulative volume of mercury intruded obtained by mercury intrusion experiments using the following equation:

$$V_{\mathrm{cp}} = V_{\mathrm{op}} - \frac{Z \times M \times (V_{\mathrm{final}} - V_{\mathrm{initial}}) \times 10^{24}}{N_A}$$

where V_{cp} and V_{op} are the volumes of the contracted and pristine open phases, respectively, expressed in Å^3, Z the number of formula per unit cell, M is the molar mass of the DUT in g.mol^{-1}, V_{final}

and $V_{initial}$ are the cumulative volumes of mercury intruded at the end and at the beginning of the transition, expressed in $mL.g^{-1}$, and N_A is Avogadro's constant in $g.mol^{-1}$.The % pressure induced volume change of the DUT can then obtained by: $\Delta V = \frac{V_{op} - V_{cp}}{V_{op}}$

9 Scanning electron microscopy

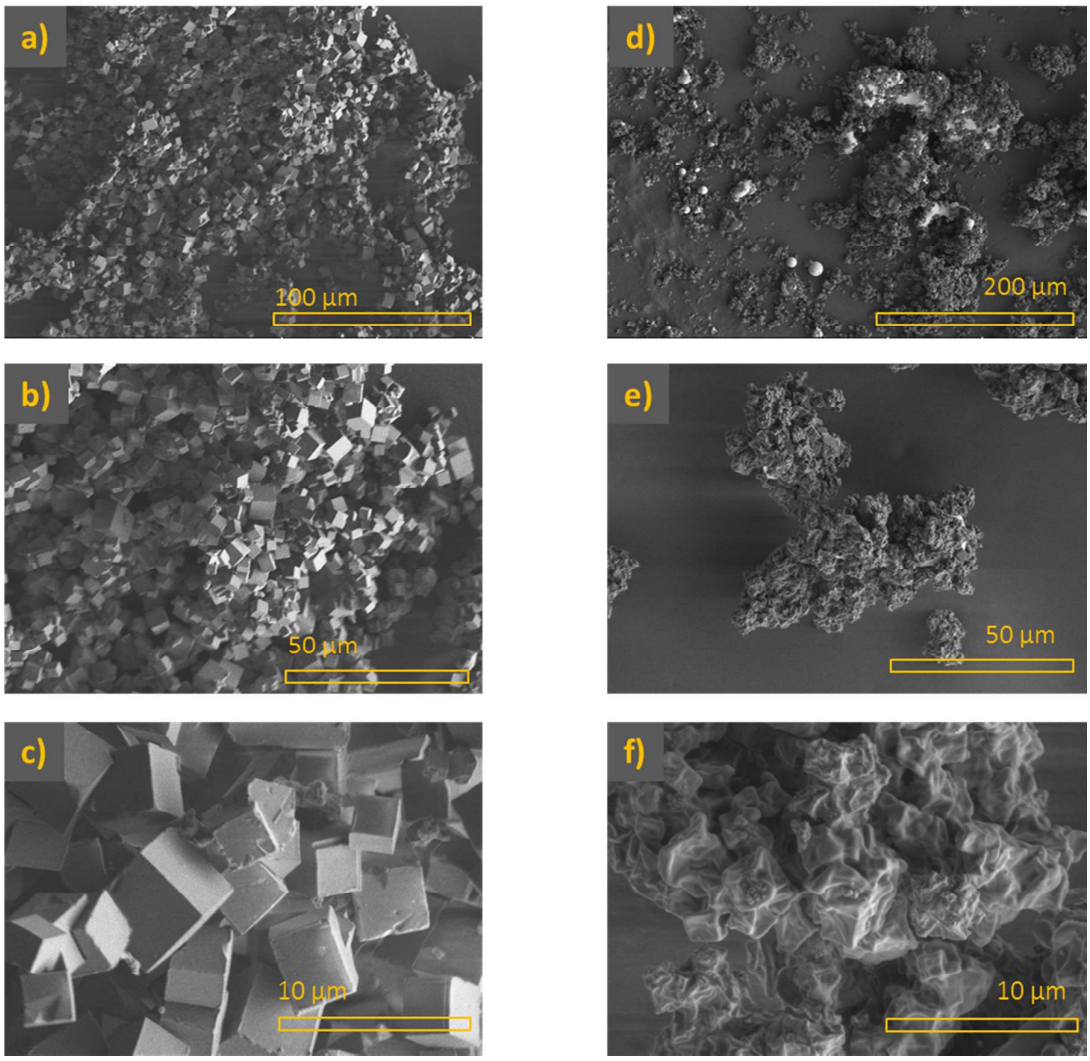

Figure S17. SEM images of DUT-49 before (a,b,c) and after (d,e,f) Hg intrusion at different magnifications.

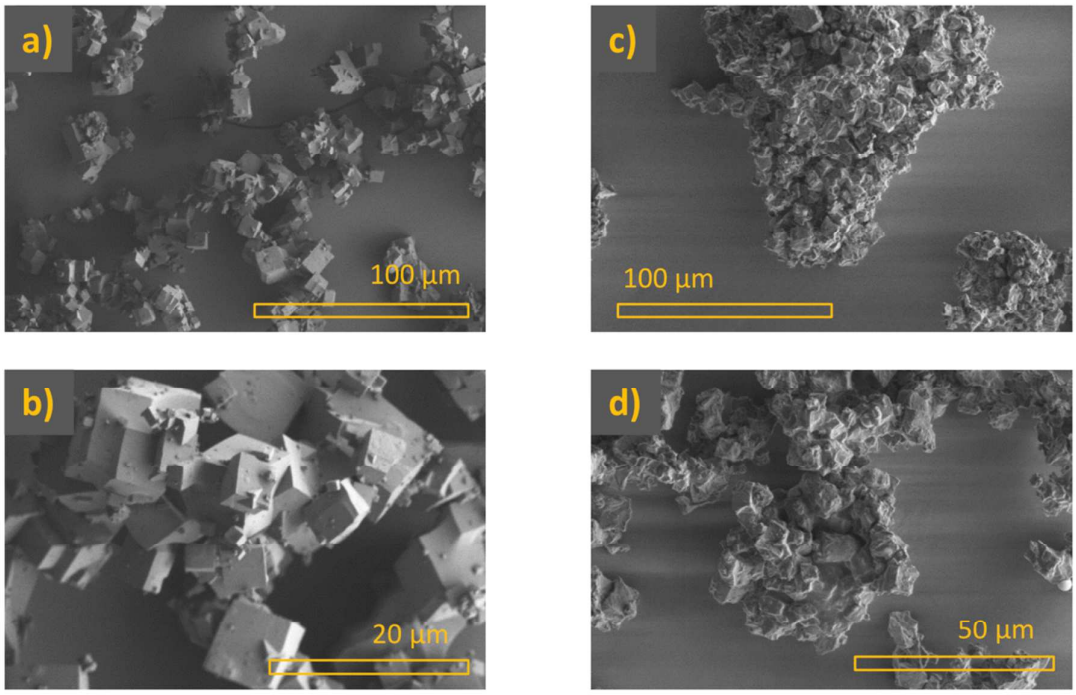

Figure S18. SEM images of DUT-48(3) before (a,b) and after (c,d) Hg intrusion at different magnifications.

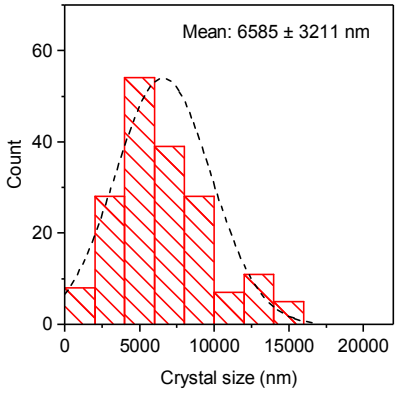

Figure S19. Crystal size distribution derived from SEM images (Figure S18) for DUT-48(3)

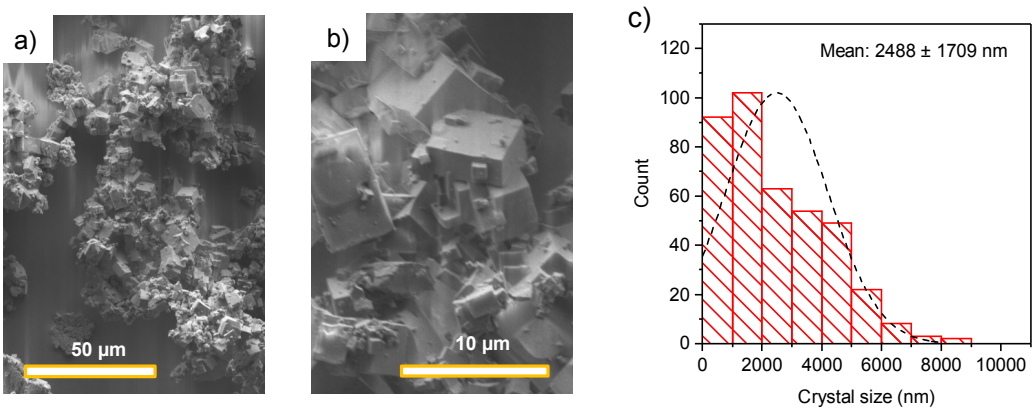

Figure S20. SEM images of DUT-48(2) (a,b) and the crystal size distribution (c).

10 Simulation of adsorption isotherms

Adsorption isotherms were simulated using the grand canonical Monte Carlo approach, implemented by the RASPA2.0 code.[10] For each adsorption pressure 5×10^5 cycles were used for equilibration and the subsequent 1×10^6 cycles were sampled. The van der Waals interactions were treated for the framework by the UFF forcefield[11] and *n*-butane the united-atom TraPPe forcefield[12] Parameters for framework—gas interactions were obtained by Lorentz-Berthelot mixing rules. No charges were considered for the framework atoms.

11 Simulation of mechanical behavior

The behavior and mechanical properties of the representative ligands were simulated for the corresponding acid via DFT optimizations using the CRYSTAL14 software[13] with localized TZVP basis sets[14] and the hybrid exchange-correlation functional PBE0[15]Long-range dispersion corrections were included via the Grimme "D2" approach[16] The ligand structure was strained by a decrease in the N–N length from the local minimum to 9.227 Å and 5.232 Å, for DUT-49 and DUT-48 respectively, in 40 steps. At each step, the structures were optimized with the N–N length fixed. Consequently, a stress-strain curve relative to this axial deformation of the ligand was generated; stress is defined by the gradient of the energy, and strain is the relative decrease in N–N length.

Classical simulations of the periodic systems used an adapted MOF-FF force field[17] by Boyd et al[18] implemented using lammps[19]. To investigate the energy landscape a series of (*N*, *V*, *T*) simulations at varying volumes *V* were conducted. Constant-volume simulations, with an initial 1 ns for equilibration and a final 1 ns for obtaining a converged value of internal pressure, were used to compute the average internal pressure for a given volume. From this series of constant-volume simulations, we integrated the internal pressure to find free-energy profiles as a function of volume.[20] All classical molecular-dynamics simulations used a time step of 1 fs and the Nosé-Hoover thermostat.[21]

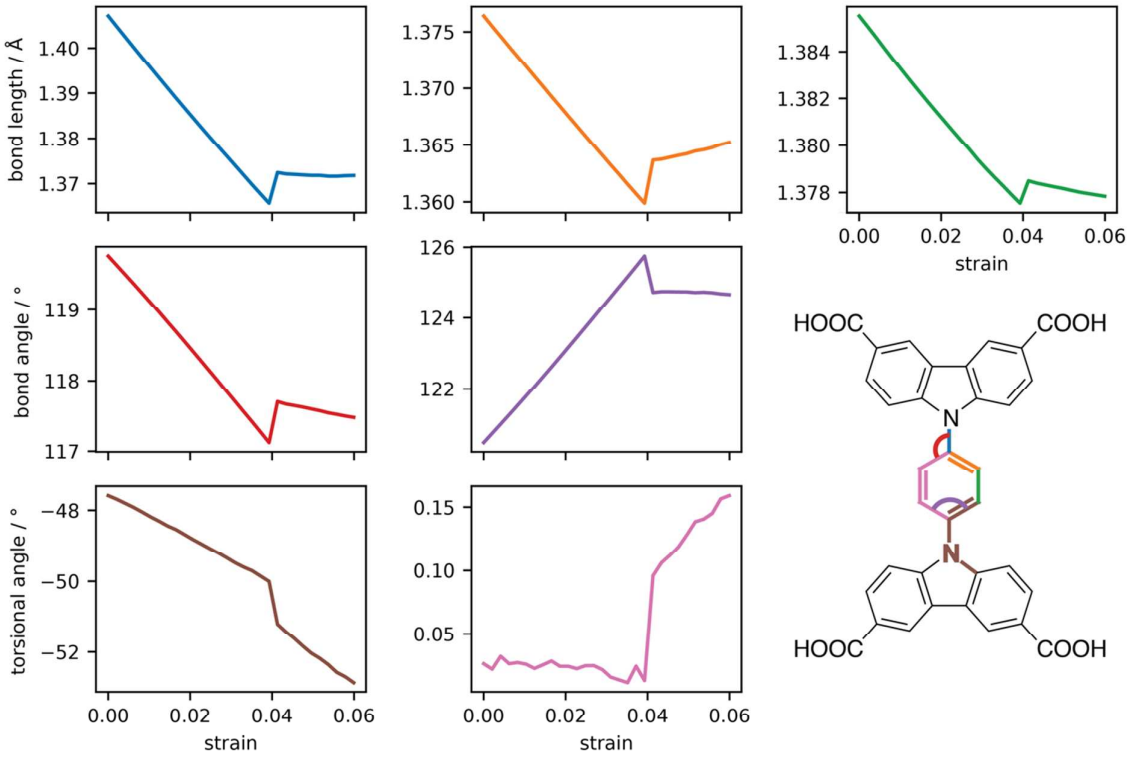

Figure S21. Evolution of key bonds, angles and dihedrals for the DUT-48 ligand under increasing compressive strain.

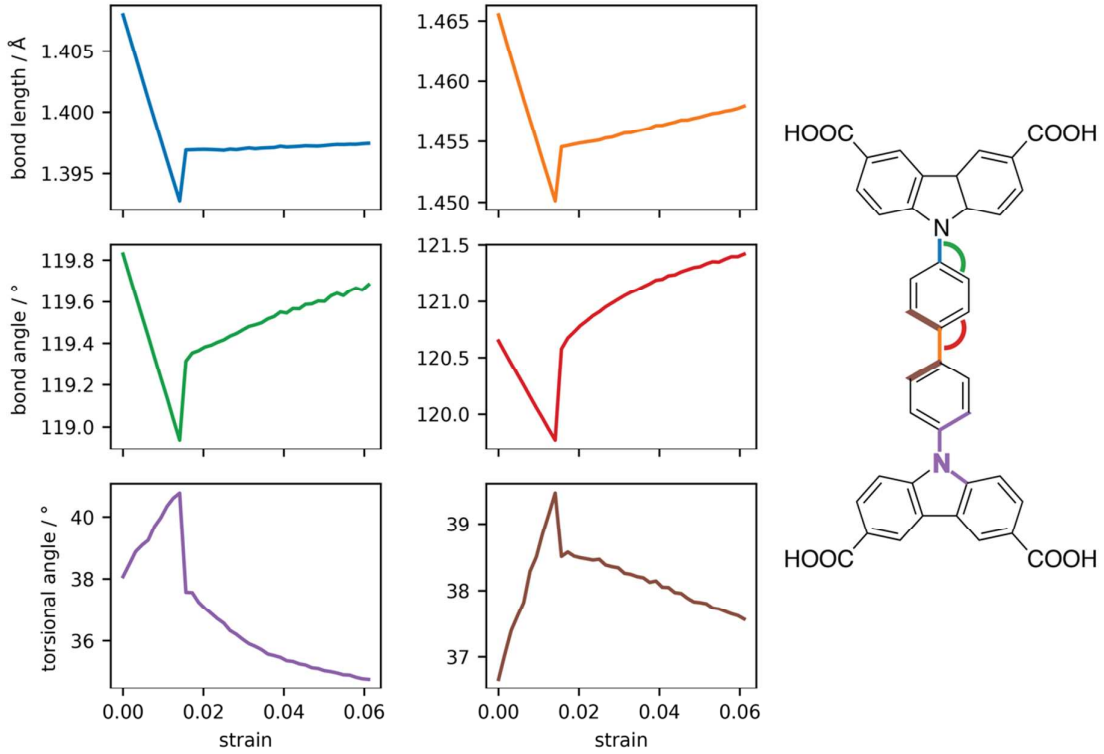

Figure S22. Evolution of key bonds, angles and dihedrals for the DUT-49 ligand under increasing compressive strain

12 Simulation of DUT-48 contracted pore structure

A structural model for DUT-48cp (contracted pore) was simulated based on the unit cell parameters derived from the mechanical MD simulations (See Fig. 5). A starting geometry was taken from of (*N*, *V*, *T*) simulations at the *cp* minima and the energy was minimized iteratively adjusting the coordinates and cell parameters using the lammps minimize and box/relax commands with default convergence criteria.

Table S3 Crystallographic data for DUT-48op, DUT-48cp, and PCN-81.

	DUT-48*op* (*exp.*)	**DUT-48*cp* (*theor.*)**	**PCN-81 (ref 2)**
Empirical formula	$C_{34}H_{20}Cu_2N_2O_{10}$	$C_{34}H_{20}Cu_2N_2O_{10}$	$C_{34}H_{20}Cu_2N_2O_{10}$
Formula weight, g mol^{-1}	743.60	743.60	743.60
Crystal system, space group	cubic, $Fm\bar{3}m$	cubic, *P1*	cubic, $Pa\bar{3}$
Unit cell dimensions, Å	*a* = 40.490(5)	*a* = 32.8	*a* = 39.4840(16)
Volume, Å^3	66381(23)	35287	61555(4)
Z	24	24	24

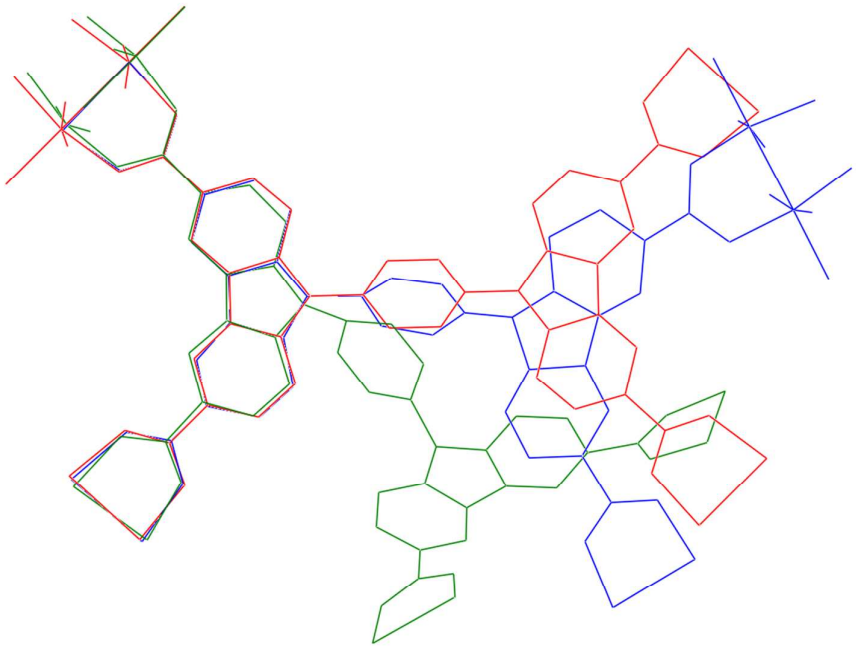

Figure S23. Comparison of linker configuration in DUT-48op (red), PCN-81 (blue), and DUT-48cp (green).

13 Author Contributions

S. Krause and U. S. synthesized and characterized the ligands and MOF materials, S. Krause, V. B. and I. S. performed adsorption experiments, V. B. measured and refined the crystal structure of DUT-48. S. E. performed SEM measurements. P. I. and P. L. L. performed and analyzed the microcalorimetry experiments. P. Y and G. M performed and analyzed the mercury intrusion experiments. S. Kaskel advised and interpreted the *in situ* characterization experiments. J. D. E. and F.-X. C. performed and interpreted the DFT, GCMC, MD simulations on DUT-48 and DUT-49. All authors contributed to writing and reviewing the manuscript.

14 References

1. Stoeck, U.; Krause, S.; Bon, V.; Senkovska, I.; Kaskel, S., A Highly Porous Metal-Organic Framework, Constructed from a Cuboctahedral Super-molecular Building Block, with Exceptionally High Methane Uptake. *Chem. Commun.* **2012**, *48* (88), 10841-10843.
2. Lu, W.; Yuan, D.; Makal, T. A.; Wei, Z.; Li, J.-R.; Zhou, H.-C., Highly Porous Metal-Organic Framework Sustained with 12-connected Nanoscopic Octahedra. *Dalton Trans.* **2013**, *42* (5), 1708-1714.
3. Krause, S.; Bon, V.; Senkovska, I.; Stoeck, U.; Wallacher, D.; Többens, D. M.; Zander, S.; Pillai, R. S.; Maurin, G.; Coudert, F.-X.; Kaskel, S., A Pressure-amplifying Framework Material with Negative Gas Adsorption Transitions. *Nature* **2016**, *532* (7599), 348-352.
4. Gerlach M.; Uwe M.; Weiss M. S., The MX Beamlines BL14.1-3 at BESSY II. *J. Large-scale Res. Facilities* **2016**, *2*, 1-6.
5. Winn, M. D.; Ballard, C.C.; Cowtan, K. D.; Dodson, E. J.; Emsley, P.; Evans, P. R.; Keegan, R. M.; Krissinel, E. B.; Leslie, A. G. W.; McCoy, A.; McNicholas, S. J.; Murshudov, G. N.; Pannu, N. S.; Potterton, E. A.; Powell, H. R.; Read, R. J.; Vagin, A.; Wilson K. S., Overview of the CCP4 Suite and Current Developments. *Acta Crystallogr. D.* **2011**, *67*, 235-242.
6. Sheldrick, G., Crystal Structure Refinement with SHELXL. *Acta Crystallogr. C* **2015**, *71*, 3-8.
7. Spek, A., Structure Validation in Chemical Crystallography. *Acta Crystallogr. D* **2009**, *65*, 148-155.
8. Llewellyn, P. L.; Maurin, G., Gas Adsorption Microcalorimetry and Modelling to Characterise Zeolites and Related Materials. *C. R. Chim.* **2005**, 8 (3), 283-302.
9. Mao, H. K.; Xu, J.; Bell, P. M., Calibration of the Ruby Pressure Gauge to 800 kbar under Quasi-hydrostatic Conditions. *J Geophy. Res. Sol. Ea.* **1986**, *91*, 4673-4676.
10. Dubbeldam, D.; Calero, S.; Ellis, D. E.; Snurr, R. Q., RASPA: Molecular Simulation Software for Adsorption and Diffusion in Flexible Nanoporous Materials. *Mol. Simulat.* **2016**, *42* (2), 81-101.
11. Rappe, A. K.; Casewit, C. J.; Colwell, K. S.; Goddard, W. A.; Skiff, W. M., UFF, a Full Periodic Table Force Field for Molecular Mechanics and Molecular Dynamics Simulations. *J. Am. Chem. Soc.* **1992**, *114* (25), 10024-10035.
12. S. Keasler, S. J.; Charan, S. M.; Wick, C. D.; Economou, I. G.; Siepmann, J. I., Transferable Potentials for Phase Equilibria–United Atom Description of Five- and Six-Membered Cyclic Alkanes and Ethers. *J. Phys. Chem. B* **2012**, *116* (36), 11234-11246..
13. Dovesi, R.; Orlando, R.; Erba, A.; Zicovich-Wilson, C. M.; Civalleri, B.; Casassa, S.; Maschio, L.; Ferrabone, M.; De La Pierre, M.; D'Arco, P.; Noël, Y.; Causà, M.; Rérat, M.; Kirtman, B., CRYSTAL14: A Program for the Ab Initio Investigation of Crystalline Solids. *Int. J. Quantum Chem.* **2014**, *114* (19), 1287-1317.
14. Peintinger, M. F.; Oliveira, D. V.; Bredow, T., Consistent Gaussian Basis Sets of Triple-zeta Valence with Polarization Quality for Solid-state Calculations. *J. Comput. Chem.* **2013**, *34* (6), 451-459.
15. Adamo, C.; Barone, V., Toward Reliable Density Functional Methods Without Adjustable Parameters: The PBE0 Model. J. Chem. Phys. 1999, 110 (13), 6158-6170.
16. Grimme, S., Semiempirical GGA-type Density Functional Constructed with a Long-range Dispersion Correction. *J. Comput. Chem.* **2006**, *27* (15), 1787-1799.
17. Bureekaew, S.; Amirjalayer, S.; Tafipolsky, M.; Spickermann, C.; Roy, T. K.; Schmid, R., MOF-FF – A Flexible First-principles Derived Force Field for Metal-Organic Frameworks. *Phys. Status Solidi B* **2013,** *250* (6), 1128-1141.
18. Boyd, P. G.; Moosavi, S. M.; Witman, M.; Smit, B., Force-Field Prediction of Materials Properties in Metal-Organic Frameworks. *J. Phys. Chem. Lett.* **2017,** *8* (2), 357-363
19. Plimpton, S., Fast Parallel Algorithms for Short-Range Molecular Dynamics. *J. Comput. Phys.* **1995,** *117* (1), 1-19.

20. Wieme, J.; Vanduyfhuys, L.; Rogge, S. M. J.; Waroquier, M.; Van Speybroeck, V., Exploring the Flexibility of MIL-47(V)-Type Materials Using Force Field Molecular Dynamics Simulations. *J. Phys. Chem. C* **2016**, *120*, 14934-14947.
21. Hoover, W. G., Canonical Dynamics: Equilibrium Phase-space Distributions. *Phys. Rev. A* **1985**, *31*, 1695-1697.